

Biotite and Muscovite $^{40}\text{Ar}/^{39}\text{Ar}$ ages from the Purcell Anticlinorium and the Kootenay Arc, Southeastern British Columbia (NTS 082F, G)

N.A. Rioseco, Department of Geoscience, University of Calgary, Calgary, Alberta, nicole.rioseco@ucalgary.ca

D.R.M. Pattison, Department of Geoscience, University of Calgary, Calgary, Alberta

A. Camacho, Department of Geological Science, University of Manitoba, Winnipeg, Manitoba

Rioseco, N.A., Pattison, D.R.M. and Camacho, A. (2020): Biotite and muscovite $^{40}\text{Ar}/^{39}\text{Ar}$ ages from the Purcell Anticlinorium and the Kootenay Arc, southeastern British Columbia (NTS 082F, G); in Geoscience BC Summary of Activities 2019: Minerals, Geoscience BC, Report 2020-01, p. 35–50.

Introduction

This paper presents new $^{40}\text{Ar}/^{39}\text{Ar}$ ages for biotite and muscovite from metasedimentary and meta-igneous rocks from the region between the towns of Creston, Kimberley and Crawford Bay in southeastern British Columbia (BC). This region comprises the interface between two major tectonic domains (Figure 1) in the southern Omineca Belt of the Canadian Cordillera: the Purcell Anticlinorium (PA) and the Kootenay Arc (KA). Geochronological data are combined with structural and metamorphic information to provide an improved understanding of the nature and significance of the interface.

The PA occupies the eastern and central portion of the study area. It is a regional-scale north-northwesterly-plunging Mesozoic fold-and-thrust structure that is cored by Mesoproterozoic rocks of the Belt-Purcell Supergroup (Price, 2000). The Belt-Purcell Supergroup comprises rift-related clastic rocks and synsedimentary mafic sills that are interpreted to have been deposited in an intracratonic rift basin between ca. 1470 and 1400 Ma (Höy, 1989; Anderson and Davis, 1995; Sears et al., 1998; Evans et al., 2000). On the eastern and western flanks of the PA, the Belt-Purcell Supergroup is unconformably overlain by the Neoproterozoic Windermere Supergroup, a sequence of rift-related clastic rocks that were deposited on the margin of ancient North America (Devlin et al., 1988; Warren, 1997; Lund et al., 2003).

In the western portion of the study area, the PA interfaces with the KA, an arcuate salient of polydeformed and polymetamorphosed rocks. The KA comprises Neoproterozoic to Paleozoic strata that were deposited on the rifted margin of ancestral North America as well as Paleozoic to Jurassic volcanic and sedimentary rocks of the Quesnel terrane that were accreted to the margin (Devlin and Bond,

1988). In general, the stratigraphy of the KA is younger than that of the PA. In the northern part of the area shown in Figure 2, the westward transition from the PA to the KA is continuous, whereas in the southern part of the area, such as in the vicinity of the town of Creston, BC, the transition is abrupt and marked by the Purcell Trench fault, which dies out going north from Creston and disappears in the vicinity of Crawford Bay.

A younging in stratigraphy between the two domains is complemented by a change in structural style, metamorphic grade and magmatism. Widespread cleavage development in the PA is stratigraphically restricted to Mesoproterozoic rocks of the Belt-Purcell Supergroup (Leech, 1962). Additionally, the PA is characterized by extensive low-grade metamorphism in the biotite zone of the greenschist facies (~450 °C and 3.5–4 kbar; Figure 2; DePaoli and Pattison, 1995; Pattison and Seitz, 2012;). In the northwestern area of Figure 2, where the transition between the PA and the KA is continuous, there is an intensification in deformation and an increase in metamorphic grade. Rocks of the KA are characterized by fabrics that are indicative of at least three Mesozoic regional-scale deformation events (Fyles, 1964; Moynihan and Pattison, 2013; Webster and Pattison, 2018). Metamorphic grade in the KA reaches upper-amphibolite facies (sillimanite+K-feldspar zone) and is marked by elongated, bull's-eye-shaped Barrovian metamorphic culmination zones (Figure 2; Moynihan and Pattison, 2013). The metamorphic grade on the eastern flank of the metamorphic culmination diminishes to that of the biotite zone, where the KA interfaces with the western flank of the PA. The KA experienced two major Mesozoic magmatic episodes resulting in the Middle Jurassic Nelson suite (Ghosh, 1995; Webster et al., 2017) and the mid- to late-Cretaceous Bayonne suite (Logan, 2001). Within the study area (Figure 2), intrusions of the Bayonne magmatic suite occur on both sides of the interface.

Papers in previous Geoscience BC reports (Rioseco and Pattison, 2018; Rioseco et al., 2019) have characterized the structural and metamorphic features of the PA and KA and the interface between them (discussed below). In this pa-

This publication is also available, free of charge, as colour digital files in Adobe Acrobat® PDF format from the Geoscience BC website: <http://www.geosciencebc.com/updates/summary-of-activities/>.

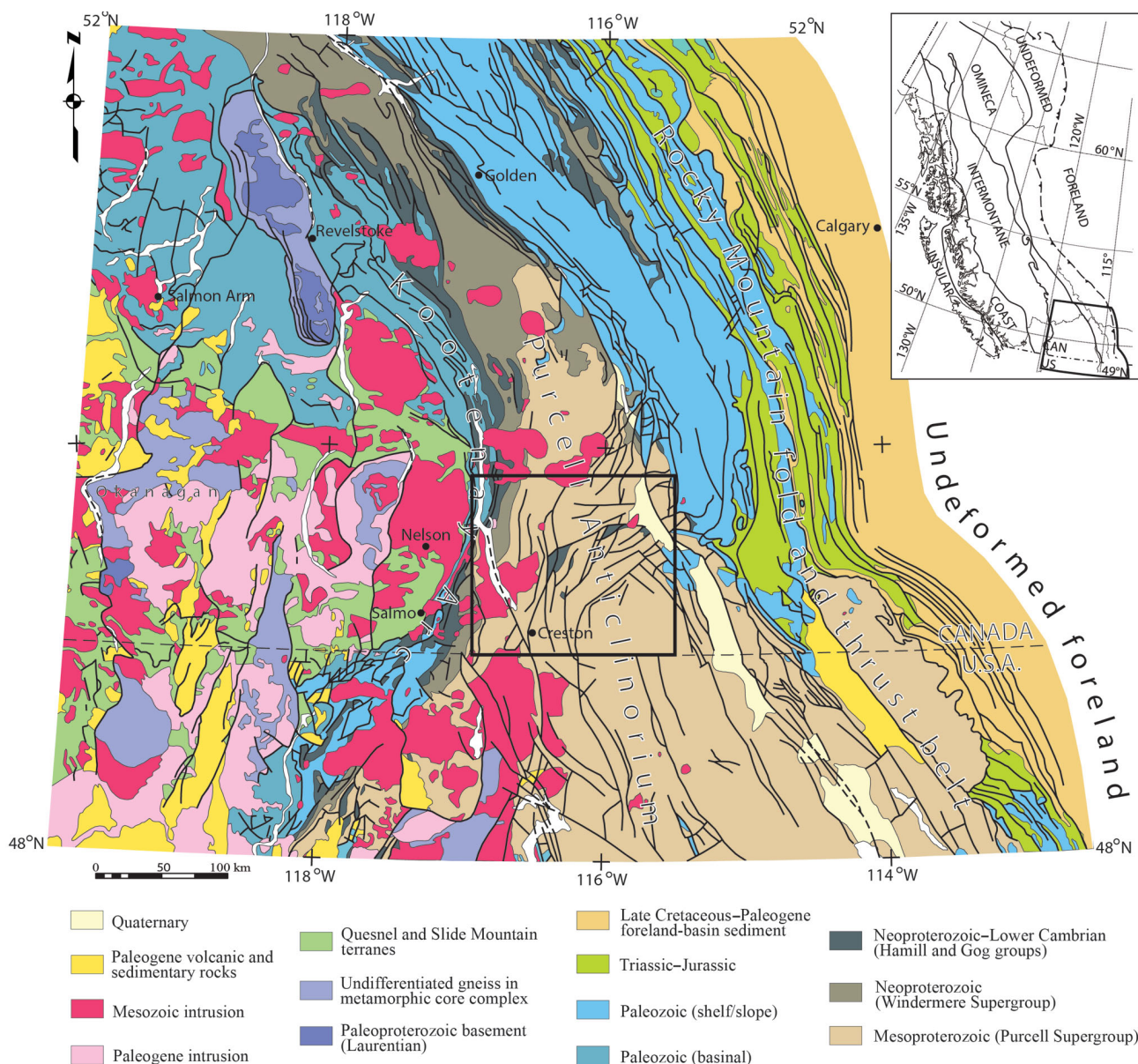


Figure 1. Regional geology of southeastern British Columbia. Geology modified from Wheeler and McFeely (1991), Moynihan and Pattison (2013) and Webster and Pattison (2018). The extent of the study area in Figures 2 and 7 is indicated by the box outlined in black.

per, new mica $^{40}\text{Ar}/^{39}\text{Ar}$ ages are presented to further constrain the nature of the two domains and their interface.

Structure and Metamorphism

Purcell Anticlinorium–type deformation is characterized by the development of penetrative slaty cleavage (S_1) that is present within argillaceous portions of turbidites of the lowermost Belt–Purcell unit. This S_1 cleavage is geographically widespread in Mesoproterozoic rocks of the PA (Figure 3a); it is not present in younger strata, indicating that it developed prior to deposition of the overlying Neoproterozoic Windermere Supergroup. The dominant Kootenay Arc–type structure is a penetrative phyllitic to fine-grained schistose foliation (S_2) that is subparallel to bedding and

dips steeply ($\sim 60^\circ$ –vertical) to the east and west (Figure 3a). Development of S_2 occurred during the second deformation phase (D_2), which is interpreted to be an Early Cretaceous deformation event (Moynihan and Pattison, 2013; Webster and Pattison, 2018) that overprinted an earlier, Mesozoic D_1 nappe-forming event.

Both the PA and KA were affected by a third episode of deformation (D_3) that is characterized by folding and the development of crenulations of S_1 or S_2 that define a spaced cleavage (S_3) and lineations (L_3). The development of S_3 and L_3 has only been observed in the northern portion of the study area (Figure 3b). The D_3 structures are thought to have developed in association with the formation of the overall anticlinorial structure of the PA and to have over-

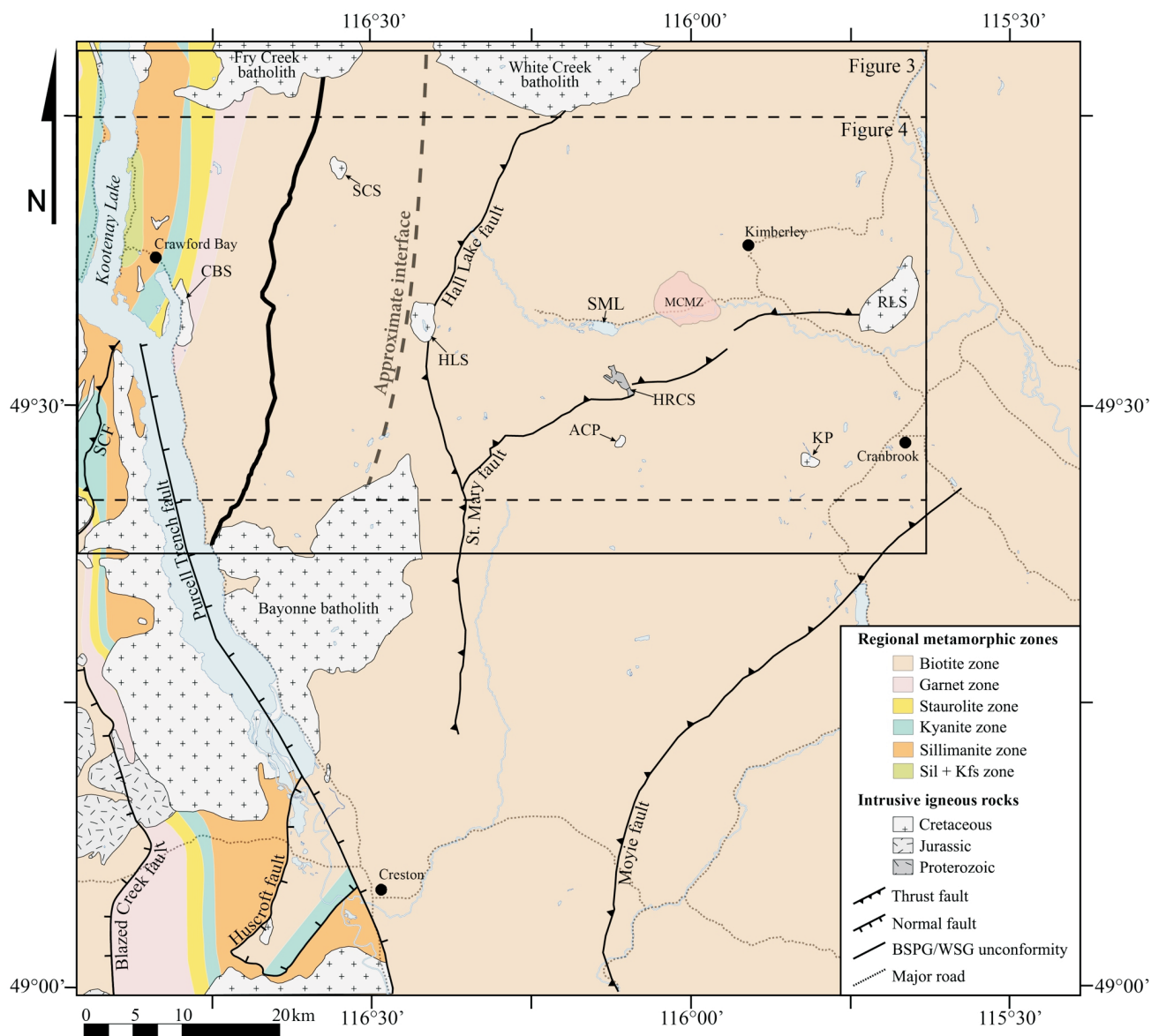


Figure 2. Distribution of metapelitic metamorphic zones within the study area (modified from Moynihan and Pattison, 2013; Webster and Pattison, 2018). The solid black outline indicates the area shown in Figures 3 and the dashed black outline indicates the area shown in Figure 4. Abbreviations: ACP, Angus Creek stock; BSPG, Belt-Purcell Supergroup; CBS, Crawford Bay stock; HLS, Hall Lake stock; Kfs, potassium feldspar; HRCS, Hellroaring Creek stock; KP, Kiakho stock; MCMZ, Matthew Creek metamorphic zone; RLS, Reade Lake stock; SCF, Seeman Creek fault; SCS, Sawyer Creek stock; Sil, sillimanite; SML, St. Mary Lake; WSG, Windermere Supergroup.

printed the D₂ structures in the KA (Price, 1984; Rioseco et al., 2019). Therefore, the structural interface between the PA and KA is best defined as the most easterly development of S₂ structures, which occurs in Belt-Purcell rocks roughly 15 km east of the unconformity between the Windermere and Belt-Purcell supergroups, at the latitude of St. Mary Lake (Figure 3).

There is no noticeable difference in metamorphic grade across the structural interface; the rocks in the PA east of the interface and the rocks on the eastern flank of the KA metamorphic culmination to the west of the interface both lie within the biotite zone (Figure 2). Therefore, a study of

mineral growth with respect to microstructures is required to identify the boundary between the PA and KA metamorphic domains. In the PA, biotite and chlorite porphyroblasts are randomly oriented in rocks that do not contain a cleavage. When S₁ is present in the rock, biotite and chlorite are aligned within the plane of S₁ (Figure 4a, b), indicating that metamorphism predated or was contemporaneous with deformation, constraining it to the Mesoproterozoic. In the KA, straight inclusion trails in biotite were inherited from S₂, indicating that biotite formed during or slightly after this event (Figure 4c–e). In addition, S₂ is folded into microlithons between the spaced-cleavage planes of S₃ (Figure 4d, e) and the path of S₃ is deflected by biotite porphyro-

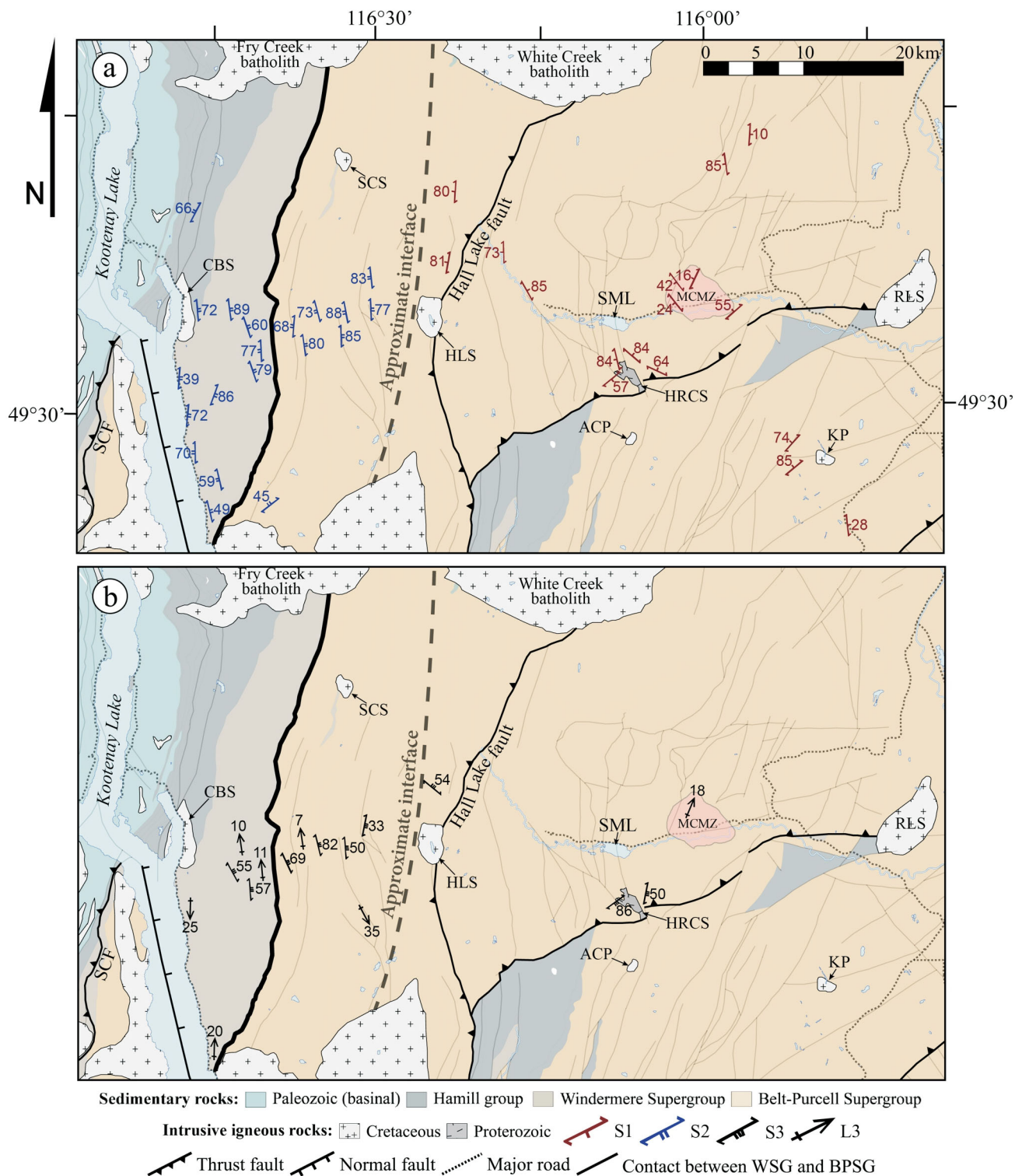


Figure 3. Distribution of structures across the northern portion of the study area: **a)** S₁ (red) and S₂ (blue) across the field area; **b)** D₃-related structures (S₃ and L₃) across the field area. Abbreviations: ACP, Angus Creek stock; BPSG, Belt-Purcell Supergroup; CBS, Crawford Bay stock; HLS, Hall Lake stock; HRCS, Hellroaring Creek stock; KP, Kiakho stock; MCMZ, Matthew Creek metamorphic zone; RLS, Reade Lake stock; SCF, Seeman Creek fault; SCS, Sawyer Creek stock; SML, St. Mary Lake; WSG, Windermere Supergroup.

blasts (Figure 4c–e). Fine-grained biotite aligned within the plane of S_2 was also subsequently deformed by D_3 (Figure 4f). The occurrence of these fabrics suggests that biotite development in this part of the KA either postdated or was approximately contemporaneous with D_2 and preceded the folding associated with D_3 . The location of the metamorphic interface defined by the change in timing of development of the biotite, as defined by the above microstructures, coincides approximately with the structural interface (Figure 4); it occurs west of the most westerly Mesoproterozoic porphyroblasts, which predate the development of S_1 , and east of the most easterly porphyroblasts that are related to Early Cretaceous D_2 deformation.

$^{40}\text{Ar}/^{39}\text{Ar}$ Thermochronology

Sample Petrography

Samples for biotite and muscovite $^{40}\text{Ar}/^{39}\text{Ar}$ geochronology were selected to provide as broad a spatial coverage as possible in the PA and across the interface with the KA. Metasedimentary rocks sampled for this study range from fine-grained quartz-mica schist and phyllite to metamorphosed argillaceous sandstone. Metamorphic grade for most samples, whether from the PA or the KA, is within the biotite zone; samples 17NR168 and 17NR169 are the exception as they come from the garnet zone. Biotite and muscovite grains in these rocks are typically <0.5 mm in size. Biotite typically occurs as randomly oriented grains in massive rocks of the PA that show no sign of S_1 (Figure 5a) and as grains that lie within the dominant schistosity (S_2) in rocks of the KA (Figure 5b). Biotite also typically contains quartz inclusions and shows some degree of chloritization, though the latter is only obvious on backscattered electron images. Care was taken when hand-picking grains to assure that those analyzed contained as few inclusions and as little chloritization as possible. Muscovite from both PA and KA samples defines the dominant schistosity (Figure 5c) but in the KA samples, muscovite is more deformed than in the PA samples (Figure 5d). Meta-igneous rocks used for this study are predominantly intermediate to mafic phases of the Moyie Sill that were emplaced in the lowermost Belt-Purcell units. Mafic sills contain the mineral assemblage amphibole(hornblende±actinolite)+plagioclase+quartz and contain variable amounts of fine-grained (~0.25 mm) biotite±chlorite±epidote (Figure 5e). Bishop (1973) described a plagioclase-quartz-biotite granophyre phase of the Moyie Sill, which lacks amphibole but contains a much greater abundance of biotite. In these rocks, biotite occurs in aggregates (individual grains range from 0.10 to 0.45 mm in size; Figure 5f).

Mineral Compositions

Mineral compositions of samples were analyzed using a JEOL Limited JXA-8200 electron-probe microanalyzer at the University of Calgary Laboratory for Electron Micro-

probe Analysis. Mineral compositions for biotite and muscovite are presented in Table 1. The Mg/(Mg+Fe) ratio across all samples is in the range of 0.31 to 0.83, with most samples clustering between 0.35 and 0.5. The F/(F+Cl+OH) ratio across all samples is between 0.00 and 0.08. There is no discernible difference between the compositions of biotite in metamorphosed igneous versus sedimentary rocks or the compositions of biotite in the metasedimentary rocks of the PA versus the KA.

$^{40}\text{Ar}/^{39}\text{Ar}$ Analytical Methods

Samples analyzed by the $^{40}\text{Ar}/^{39}\text{Ar}$ method were crushed using standard rock-crushing techniques and micas were separated from the bulk of the sample on a shaking table. Grains were then sieved, washed and subsequently hand picked. Separated grain sizes typically ranged from 250 to 297 μm , but larger (297–420 μm) grains were picked when possible and smaller (<250 μm) grains, when necessary.

The following methodology is reproduced from the supplementary material provided by Larson et al. (2017):

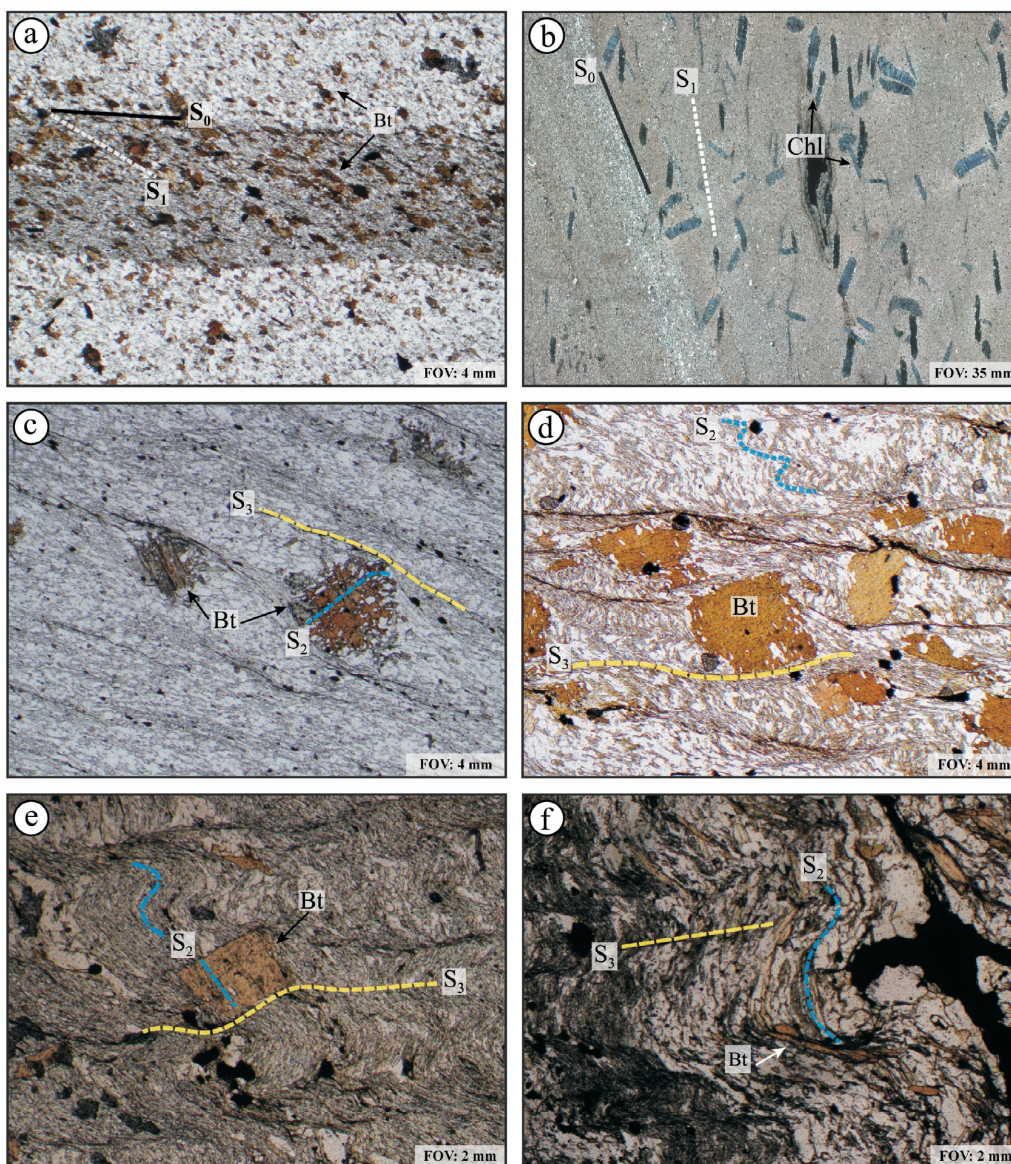
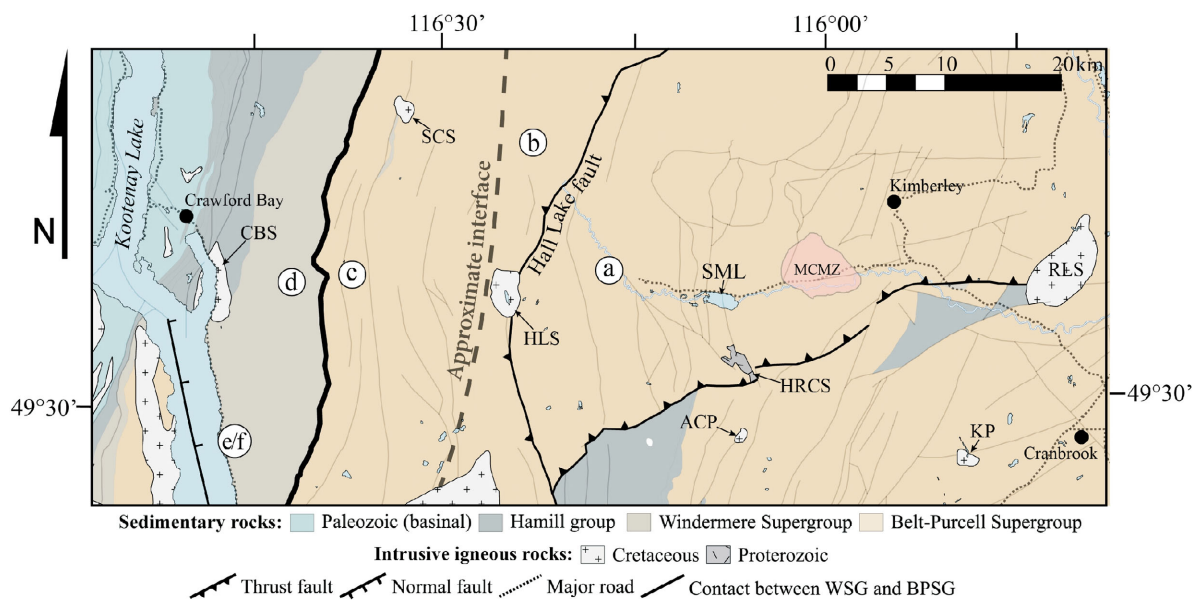
“The $^{40}\text{Ar}/^{39}\text{Ar}$ analytical work was performed at the University of Manitoba using a multi-collector Thermo Fisher Scientific ARGUS VI mass spectrometer, linked to a stainless steel Thermo Fisher Scientific extraction/purification line and Photon Machines (55 W) Fusions 10.6 CO₂ laser. Argon isotopes (from mass 40–37) were measured using Faraday detectors with low noise $1 \times 10^{12} \Omega$ resistors and mass 36 was measured using a compact discrete dynode (CDD) detector. The sensitivity for argon measurements is $\sim 6.312 \times 10^{17}$ moles/fA as determined from measured aliquots of Fish Canyon Sanidine (Dazé et al., 2003; Kuiper et al., 2008).”

Standards and unknowns were placed in 2-mm-deep wells in 18-mm-diameter Al disks, with standards placed strategically so that the lateral neutron flux gradients across the disk could be evaluated. Planar regressions were fit to the standard data, and the $^{40}\text{Ar}/^{39}\text{Ar}$ neutron fluence parameter, J , was interpolated for the unknowns. Uncertainties in J are estimated at 0.1–0.2% (1 σ), based on Monte Carlo error analysis of the planar regressions (Best et al., 1995). All specimens were irradiated in the Cd-lined, in-core CLICIT facility of the Oregon State University TRIGA reactor (Corvallis, Oregon, USA).”

The duration of irradiation was 20 hours and included Fish Canyon sanidine (28.2 Ma; Kuiper et al., 2008) and GA1550 biotite (98.5 Ma; Spell and McDougall, 2003) reference standards.

“Irradiated samples were placed in a Cu sample tray, with a KBr cover slip, in a stainless steel high vacuum extraction line and baked with an infrared lamp for 24 hours. Single crystals were either fused...”

or step-heated



“...using the laser, and reactive gases were removed, after ~3 minutes, by three NP-10 SAES getters (two at room temperature and one at 450 °C) prior to being admitted to the mass spectrometer by expansion. Five argon isotopes were measured simultaneously over a period of 6 min. Measured isotope abundances were corrected for extraction line blanks, which were determined before every sample analysis.”

Line blanks averaged ~5.77 fA for mass 40 and ~0.02 fA for mass 36.

Detector intercalibration (IC) between the different faraday cups (H1 = ^{40}Ar , AX = ^{39}Ar , L1 = ^{38}Ar , L2 = ^{37}Ar) was monitored (in Qtegra) every four days by peak hopping ^{40}Ar . Calculated values are ICH1: 1.0000, ICAX: 1.0745, ICL1: 1.0637 and ICL2: 1.0534, with an error of approximately 0.2%. The intercalibration factor between H1 and the CDD was measured with the unknowns resulting in ICCDD: 1.0056 ± 0.0006 per atomic mass unit. Additionally, as outlined in Larson et al. (2017):

“A value of 295.5 was used for the atmospheric $^{40}\text{Ar}/^{36}\text{Ar}$ ratio (Steiger and Jager, 1977) for the purposes of routine measurement of mass spectrometer discrimination using air aliquots, and correction for atmospheric argon in the $^{40}\text{Ar}/^{39}\text{Ar}$ age calculation. Corrections are made for neutron-induced ^{40}Ar from potassium, ^{39}Ar and ^{36}Ar from calcium, and ^{36}Ar from chlorine (Roddick, 1983; Renne et al., 1998; Renne and Norman, 2001).”

Data collection was performed using Pychron software (Ross, 2017), and data reduction, error propagation, age calculation and plotting were performed using MassSpec software (version 8.091; Deino, 2013). The decay constants used were those recommended by Steiger and Jager (1977).

Criteria for Defining Ages

Argon release patterns for micas analyzed in this study are complex and they fall into five groups: 1) age spectra that define plateaus (Figure 6a), 2) relatively flat age spectra with ‘forced plateaus’ (Figure 6b), 3) monotonically increasing age spectra (Figure 6c), 4) half-saddle-shaped age spectra (Figure 6d), and 5) relatively flat age spectra, in which large portions of the ^{39}Ar were released in single

steps (Figure 6e, f). As a result, interpreted ages presented in Table 2 represent a best estimate of the cooling age. A distinction is made between a date and an age in that a date lacks any sort of significance, whereas the term ‘age’ is reserved for what is interpreted to be in some way significant. Isoplot (Ludwig, 2008) was used to calculate plateau ages and the criteria set for a plateau was three or more contiguous steps, representing >50% ^{39}Ar released, with dates that are within uncertainty of each other at the 2σ level (Dalrymple and Lanphere, 1974; Lee et al., 1991). However, several samples did not meet these criteria.

An ‘interpreted age’ resulting from a forced plateau was calculated from three or more consecutive steps that produce a relatively flat profile but do not overlap in uncertainty at the 2σ level. In the cases where the step dates do not define a plateau or forced plateau, the interpreted age is an ‘integrated age’, which is determined by weighing the dates of the individual steps by the fraction of ^{39}Ar released. Calculation of an integrated age was typically reserved for experiments where a large portion of ^{39}Ar was released in a single step.

Half-saddle-shaped age spectra are characterized by a pattern of high initial $^{40}\text{Ar}/^{39}\text{Ar}$ dates that decrease to a trough at the end of the spectrum. This type of Ar-release pattern is interpreted as reactor-induced recoil loss of ^{39}Ar . Lanphere and Dalrymple (1976) suggested that the step or average of multiple steps comprising the trough of the saddle results in the best estimate of an age for the mineral. In this study, the age spectra with troughs consisting of fewer than three are considered as having no plateau. The interpreted age is determined from the step or steps in the trough that define a plateau segment; plateau segments defined in this study comprise between 15 and 40% of the total ^{39}Ar released.

Biotite and muscovite results will be discussed together in the following sections. For clarity, sample numbers that correspond to muscovite will be followed by ‘-Ms’.

Results and Interpretation

The $^{40}\text{Ar}/^{39}\text{Ar}$ ages obtained from rocks in the PA, east of the structural and metamorphic interface, have been subdivided into three domains separated by major north-north-east-trending thrust faults (Figure 1): the Moyie and the St.

Figure 4. Photomicrographs from across the structural and metamorphic interface, along with a map (top) indicating sample locations (letters match those identifying the photomicrographs): **a)** biotite-bearing metasediment from the Aldridge Formation, with biotite randomly oriented in arenaceous beds and aligned within the plane of S_1 in argillaceous parts of the rock; **b)** Aldridge Formation metasediments, with randomly oriented chlorite porphyroblasts that have been deformed in the orientation of S_1 ; **c)** argillaceous sandstone of the Dutch Creek Formation, in which biotite contains inclusion trails that are interpreted to have been inherited from S_2 and S_3 cleavage wraps around biotite porphyroblasts; **d)** crenulated fine-grained schist from the Horsethief Creek Group, with biotite porphyroblasts that predate the development of S_3 ; **e)** crenulated phyllite from the Horsethief Creek Group, with biotite porphyroblasts that predate the development of S_3 ; **f)** crenulated phyllite from the Horsethief Creek Group, with fine-grained biotite within the primary foliation plane (S_2) that predates the development of S_3 . All samples are shown under plane-polarized light. Abbreviations: ACP, Angus Creek stock; BPSG, Belt-Purcell Supergroup; Bt, biotite; CBS, Crawford Bay stock; Chl, chlorite; HLS, Hall Lake stock; HRCS, Hellroaring Creek stock; FOV, field of view; KP, Kiakho stock; MCMZ, Matthew Creek metamorphic zone; RLS, Reade Lake stock; SCF, Seeman Creek fault; SCS, Sawyer Creek stock; SML, St. Mary Lake; WSG, Windermere Supergroup.

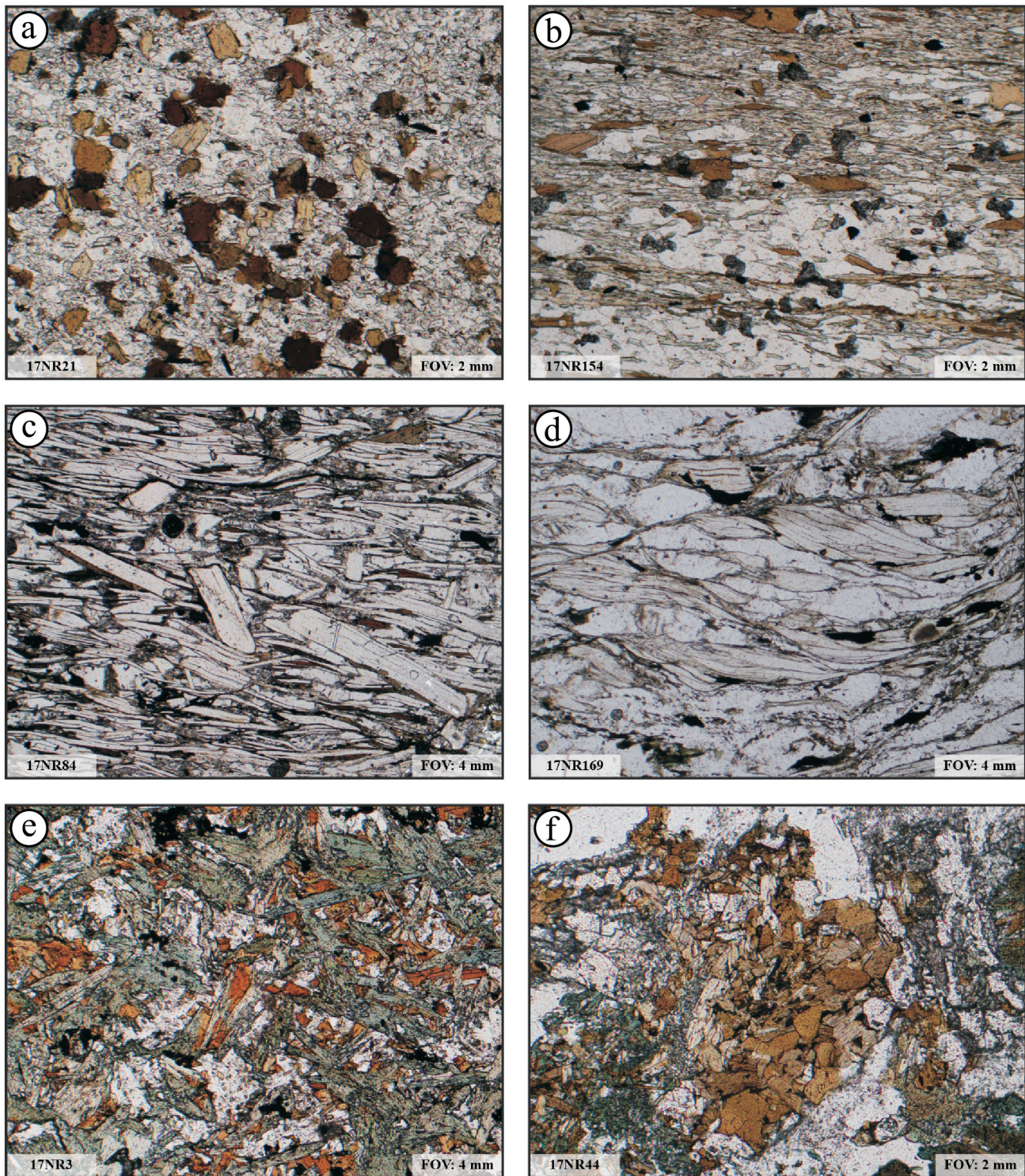


Figure 5. Representative photomicrographs of samples from the study area analyzed by the $^{40}\text{Ar}/^{39}\text{Ar}$ method: **a)** biotite-bearing metasediments from the middle Aldridge Formation near Yahk, BC; **b)** biotite-bearing fine-grained schist from the Horsethief Creek Group east of Gray Creek, BC; **c)** fine-grained muscovite schist of the lower Aldridge Formation from near the Hellroaring Creek stock; **d)** fine-grained muscovite schist of the Hamill group from near Crawford Bay, BC; **e)** metagabbro of the Moyie Sill, northeast of Yahk, BC; **f)** granophyre phase from the Moyie Sill, east of Creston, BC. Abbreviation: FOV, field of view.

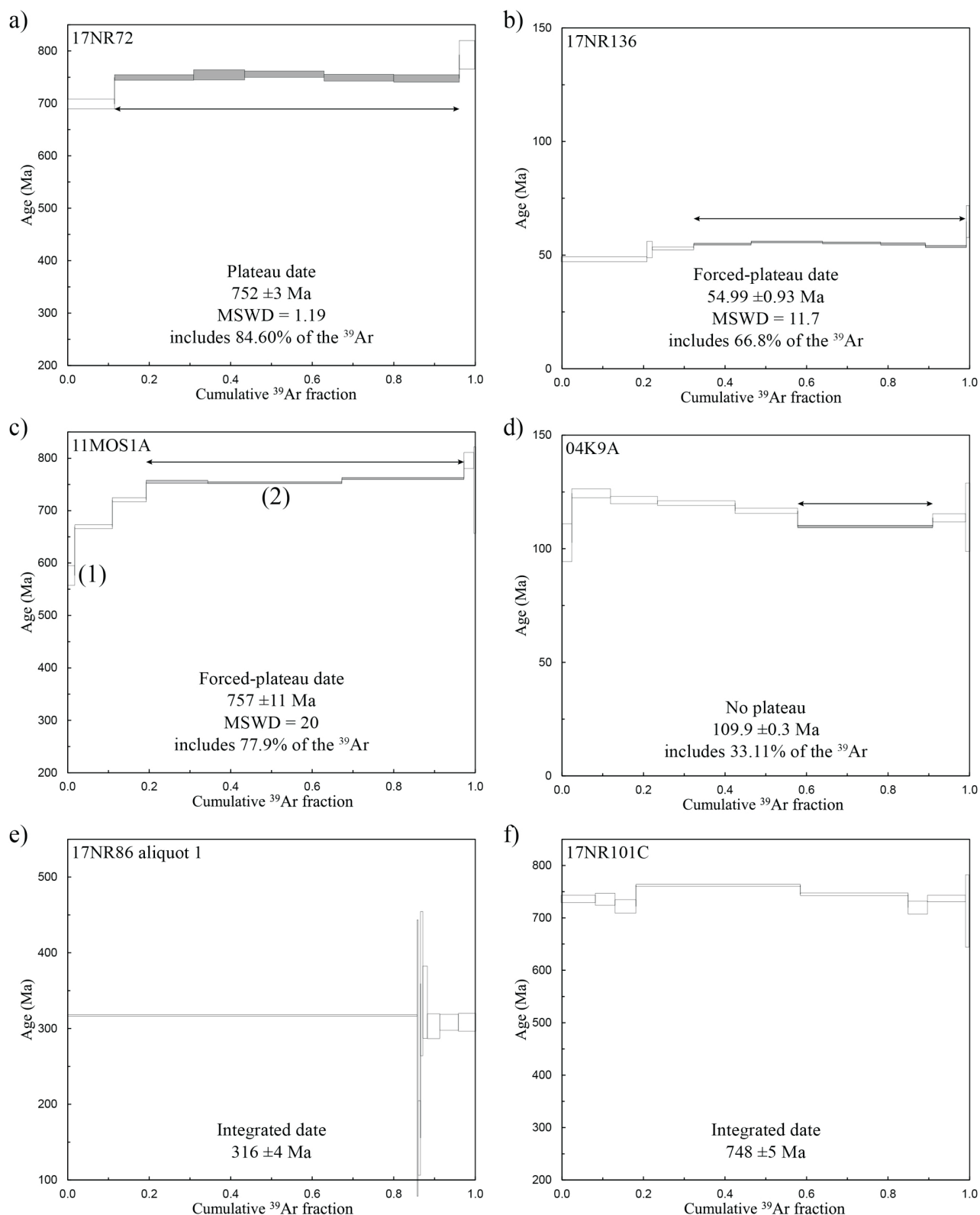


Figure 6. Representative $^{40}\text{Ar}/^{39}\text{Ar}$ age spectra for select samples from the study area: **a)** plateau date for sample 17NR72 from near Yahk, BC; **b)** forced plateau from a relatively flat age spectrum from near Boswell, BC; **c)** forced plateau from a monotonically increasing age spectrum from east of Yahk, BC, where point 2 indicates the best estimate for the age of the sample and point 1 indicates the time of final closure to argon diffusion; **d)** half-saddle-shaped spectrum, in which the age is interpreted from the results in the trough at the end of the spectrum; **e)** relatively flat spectrum with a large portion of ^{39}Ar released in a single step from near the Hellroaring Creek stock; **f)** relatively flat spectrum with a calculated integrated age from within the Matthew Creek metamorphic zone. Abbreviation: MSWD, mean square of weighted deviates.

Table 2. Summary of ⁴⁰Ar/³⁹Ar results (where n is the number of grains analyzed) from the study area. Abbreviations: Bt, biotite; Fm., Formation; FP, forced plateau; I, integrated date; Ms, muscovite; MSWD, mean square of weighted deviates; NP, no plateau; P, plateau. Unless otherwise noted, error is reported at the 2σ level.

Sample	Easting	Northing	Unit	Rock type	Mineral analyzed	Grain diameter (μm)	n	Date (Ma)	³⁹ Ar fraction	Age spectrum			Type	J value	±1σ
										MSWD	Integrated date (Ma)	Interpreted age (Ma)			
04K9A	515505	548328	Horsethief Creek Fm.	Metasediment	Bt	<250	5	109.9 ±0.3	33.11	N/A	115.81 ±1.57	109.9 ±0.3	NP	5.32E-03	3.76E-06
08MC3A	565318	5495890	Aldridge Fm.	Metasediment	Bt	297-250	4	432 ±5	18.11	N/A	496 ±5	432 ±5	NP	5.33E-03	2.28E-06
11MOS1A	584333	5439814	Aldridge Fm.	Metasediment	Bt	297-250	3	757 ±11	77.90	20	744 ±3	757 ±11	FP	5.29E-03	3.62E-06
12MS20	547277	5444841	Moyie Sills	Granophyre	Bt	420-297	2	366 ±8	36.70	4.1	377 ±5	366 ±8	FP	5.29E-03	3.55E-06
17NR3	572345	5449092	Moyie Sills	Mafic	Bt	297-250	2	489 ±2	70.22	N/A	567 ±7	489 ±2	NP	5.28E-03	6.52E-06
17NR6	548155	5444349	Moyie Sills	Granophyre	Bt	297-250	2	-	-	-	633 ±14	~600	NP	5.28E-03	4.32E-06
17NR14B	556865	5429592	Aldridge Fm.	Granodiorite	Bt	420-297	2	82.42 ±0.89	58.15	2	78.20 ±2.25	82.42 ±0.89	FP	5.28E-03	2.87E-06
17NR21	565449	5437346	Aldridge Fm.	Metasediment	Bt	<250	2	837 ±13	95.20	1.6	824 ±42	837 ±13	P	5.29E-03	6.06E-06
17NR44	541523	5439802	Moyie Sills	Granophyre	Bt	297-250	2	606 ±17	88.40	8.9	610 ±14	606 ±17	FP	5.29E-03	6.06E-06
17NR45	542208	5440222	Aldridge Fm.	Metasediment	Bt	<250	3	305 ±2	89.61	N/A	306 ±10	305 ±2	NP	5.30E-03	5.32E-06
17NR72	570325	5439259	Moyie Sills	Mafic	Bt	297-250	3	752 ±3	84.60	1.19	749 ±9	752 ±3	P	5.31E-03	6.04E-06
17NR86 aliquot 1	558368	5490387	Aldridge Fm.	Metasediment	Bt	297-250	2	-	-	-	316 ±4	316 ±4	I	5.28E-03	3.53E-06
17NR86 aliquot 2	558368	5490387	Aldridge Fm.	Metasediment	Bt	297-250	2	240.60 ±3.4	23.70	2.4	265 ±5	240 ±3	FP	5.28E-03	3.53E-06
17NR132	570840	5498230	Aldridge Fm.	Metasediment	Bt	297-250	4	582 ±15	40.40	7.8	668 ±10	582 ±15	FP	5.32E-03	4.14E-06
17NR136	517814	5475451	Horsethief Creek Fm.	Metasediment	Bt	707-420	1	54.99 ±0.93	66.80	11.7	53.41 ±0.68	54.99 ±0.93	FP	5.31E-03	4.18E-06
17NR154	520954	5496147	Horsethief Creek Fm.	Metasediment	Bt	297-250	4	-	-	-	84.04 ±2.75	84.04 ±2.75	NP	5.33E-03	4.77E-06
17NR160	523416	5492041	Horsethief Creek Fm.	Metasediment	Bt	297-250	4	139.8 ±1.6	96.50	13	139.23 ±1.06	139.8 ±1.6	FP	5.32E-03	3.56E-06
17NR161	525329	5495116	Dutch Creek Fm.	Metasediment	Bt	297-250	3	64.1 ±1.8	90.70	15	62.61 ±1.13	64.1 ±1.8	FP	5.32E-03	4.98E-06
12HRC2A	560553	5490222	Aldridge Fm.	Metasediment	Ms	707-420	1	704 ±2	83.50	2.7	700 ±6	704 ±2	FP	5.32E-03	4.10E-06
17NR84 aliquot 1	559419	5492015	Aldridge Fm.	Metasediment	Ms	420-297	2	-	-	-	674 ±6	674 ±6	I	5.28E-03	3.83E-06
17NR84 aliquot 2	559419	5492015	Aldridge Fm.	Metasediment	Ms	420-297	3	-	-	-	524 ±6	524 ±6	I	5.28E-03	3.83E-06
17NR101C	566235	5499982	Aldridge Fm.	Metasediment	Ms	420-297	3	-	-	-	748 ±5	748 ±5	I	5.33E-03	4.79E-06
17NR168 aliquot 1	516540	5506707	Hamill group	Metasediment	Ms	420-297	4	-	-	-	79.82 ±1.14	79.82 ±1.14	I	5.32E-03	4.27E-06
17NR168 aliquot 2	516540	5506707	Hamill group	Metasediment	Ms	420-297	3	-	-	-	77.68 ±1.14	77.68 ±1.14	I	5.32E-03	4.27E-06
17NR169	516614	5506727	Hamill group	Metasediment	Ms	420-297	3	-	-	-	83.60 ±0.89	83.60 ±0.89	I	5.33E-03	2.59E-06

Mary–Hall Lake faults. The southeastern domain is in the footwall of the Moyie fault. The western domain occurs between the Moyie and St. Mary faults, with data coming from its western portion near the town of Creston, BC, in the immediate hangingwall of the Purcell Trench fault. The northern domain is bounded by the St. Mary and Hall Lake faults in the vicinity of St. Mary Lake. The KA, more specifically rocks west of the structural and metamorphic interface, is referred to as a single domain. Representative age spectra are presented in Figure 6 and $^{40}\text{Ar}/^{39}\text{Ar}$ results are summarized in Table 2.

Four biotite separates from the eastern domain were analyzed in this study. Two samples, 17NR21 and 17NR72 returned plateau ages interpreted at 837 ± 13 Ma and 752 ± 3 Ma (Figure 6a), respectively. Sample 11MOS1A yielded a monotonically increasing spectrum with an ‘forced plateau’ age of 757 ± 11 Ma (Figure 6c). This type of age spectrum is typically interpreted to reflect argon loss either to partial resetting (time point 1; ~580 Ma) or protracted cooling (between time points 2 [~757 Ma] and 1 [~580 Ma]; McDougall and Harrison, 1999). In the fourth sample, 17NR3, a large portion (>70%) of the ^{39}Ar was released in a single step, so an integrated age of 489 ± 2 Ma is reported for this sample.

Four biotite separates from the western domain near the town of Creston yielded $^{40}\text{Ar}/^{39}\text{Ar}$ ages between ca. 305 and ca. 606 Ma. Sample 17NR44 returned a forced-plateau age of 606 ± 17 Ma, whereas sample 17NR6 (~600 Ma) is characterized by a half-saddle-shaped spectrum. Samples 17NR45 and 12MS20 yielded integrated ages of ca. 305 Ma and ca. 366 Ma, respectively. Biotite separates from a small, unmapped tonalitic intrusive body (17NR14B) located in the hangingwall of the Moyie fault (~2 km from the fault trace) returned a forced plateau age of 82 ± 1 Ma. This age is interpreted from a monotonically increasing spectrum that indicates final closure to Ar loss at approximately 25 Ma. The significance of this sample will be discussed further below.

Mica from six samples from the northern domain were dated by $^{40}\text{Ar}/^{39}\text{Ar}$: three muscovites and three biotites. Sample 17NR101C-Ms does not yield a plateau; the integrated age is 748 ± 5 Ma (Figure 6f). The age spectrum for sample 12HRC2A-Ms monotonically increases from ca. 105 Ma in the low-temperature steps to ca. 704 Ma in the higher temperature steps. Two aliquots of muscovite from sample 17NR84-Ms did not return age plateaus; the integrated age for aliquot 1 is 674 ± 6 Ma and that for aliquot 2 is 524 ± 6 Ma. Petrographic observations indicate that there may be two populations of muscovite in this sample (Figure 5c); however, the inconsistency between the two aliquots renders the significance of this age uncertain. Biotite-cooling ages from the northern domain are typically characterized by a half-saddle shape (17NR132: ca.

582 Ma; 08MC3A: ca. 432 Ma; 17NR86 [aliquot 2]: 240 Ma). The first aliquot analyzed for sample 17NR86 (aliquot 1) returned an integrated cooling age of 316 ± 4 Ma (Figure 6e), significantly older than the second aliquot; however, unlike the muscovite in sample 17NR84-Ms, there is no evidence of two populations of biotite. The variation in cooling ages across aliquots will be addressed further below.

Mica cooling ages for the KA are much younger than those from the PA, between ca. 139 and ca. 55 Ma. In this region, two muscovite samples (17NR168-Ms, comprising two aliquots, and 17NR169-Ms) produced age spectra, in which a large portion of ^{39}Ar was released in a single step. Nevertheless, spectrum profiles are relatively flat so an integrated age was calculated for each; the two aliquots of separates for 17NR168 returned similar ages of 79.8 ± 1.1 Ma and 77.7 ± 1.1 Ma, whereas 17NR169 yielded an age of 83.6 ± 0.9 Ma. Three of the five biotite samples returned forced-age plateaus from relatively flat spectra; (17NR160: 139 ± 1.6 Ma, 17NR161: 64 ± 1.8 Ma, 17NR136: 55 ± 0.93 Ma; Figure 6b). The interpreted age for 04K9A is ca. 110 Ma from a half-saddle-shaped spectrum (Figure 6d). Sample 17NR154 did not return a plateau, so the calculated integrated date (84 ± 2.75 Ma) is the interpreted age for this sample.

Discussion

$^{40}\text{Ar}/^{39}\text{Ar}$ Ages in the Purcell Anticlinorium

The significance of each individual cooling age in the PA is difficult to assess due to complex Ar-diffusion profiles of individual analyses and the nonsystematic distribution of ages across the PA (Figure 7). Several processes, individually or collectively, may have influenced the cooling history observed in the age spectra associated with rocks from the PA. The Belt–Purcell Supergroup was affected by three tectonic events prior to deposition of the Neoproterozoic Windermere Supergroup. These include: 1) the ca. 1350 Ma East Kootenay orogeny, which has been recognized as an extensional event (Anderson and Davis, 1995; Doughty and Chamberlain, 1996; McFarlane, 2015); 2) a cryptic, Grenville-age event that resulted in ca. 1100–1000 Ma U–Pb ages in metamorphic zircon, monazite and titanite (Anderson and Davis, 1995; Doughty and Chamberlain, 1996; McFarlane, 2015); and 3) the ca. 900–800 Ma Goat River orogeny, which was described by McMechan and Price (1982) as a period of uplift and block faulting. Following the deposition of the Windermere Supergroup, the region was differentially uplifted and eroded, both of which were interpreted to have been caused by the rifting of Rodinia. The Montania (Deiss, 1941; Norris and Price, 1966; Benvenuto and Price, 1979) and Windermere highs (Price, 2000) are two of several topographic ‘highs’, or regions of high topographic relief, that

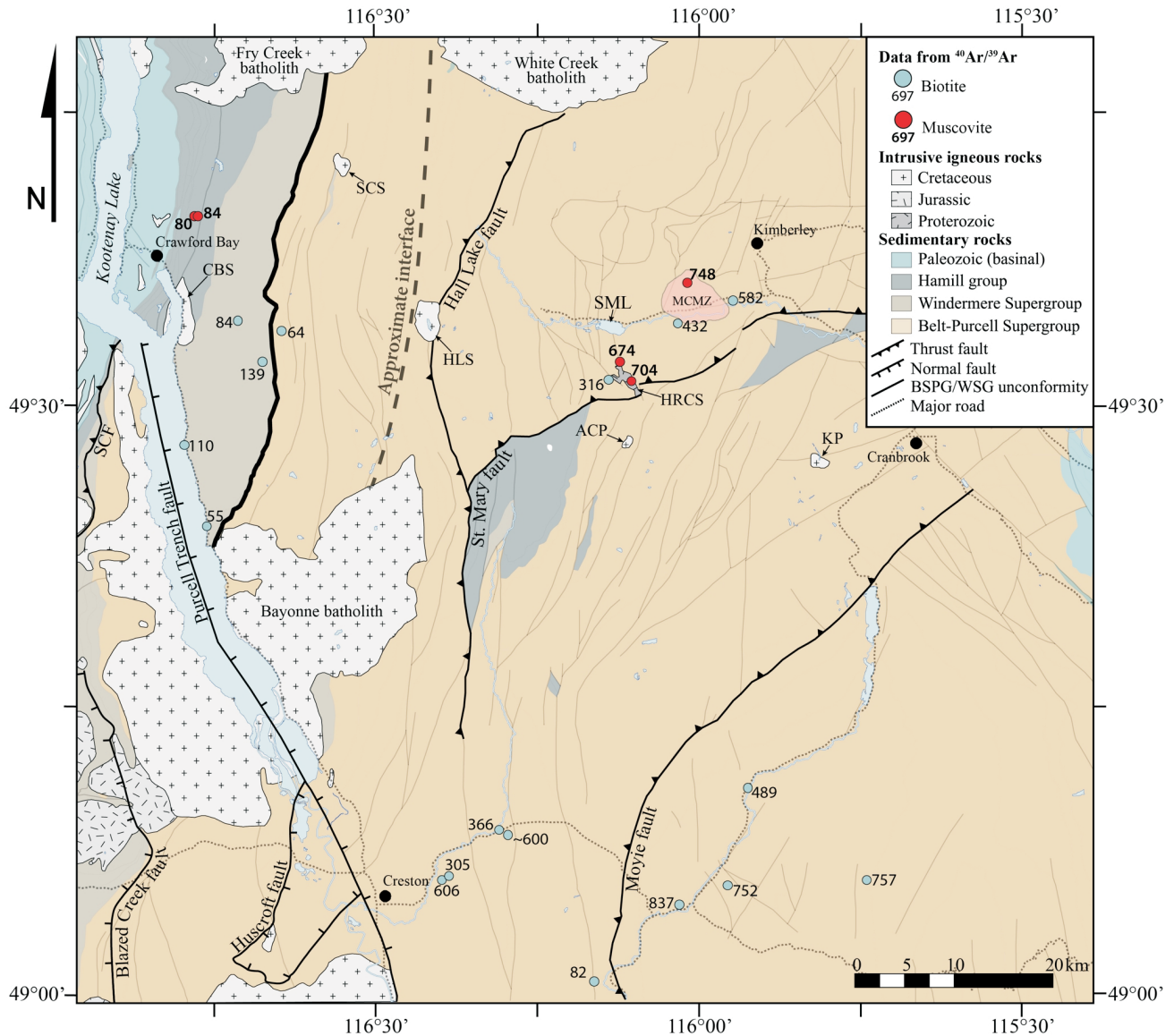


Figure 7. Map of $^{40}\text{Ar}/^{39}\text{Ar}$ mica cooling ages (reported in Ma) from the study area. Abbreviations: ACP, Angus Creek stock; BSPG, Belt-Purcell Supergroup; CBS, Crawford Bay stock; HLS, Hall Lake stock; HRCS, Hellowroaring Creek stock; KP, Kiakho stock; MCMZ, Matthew Creek metamorphic zone; RLS, Reade Lake stock; SCF, Seeman Creek fault; SCS, Sawyer Creek stock; SML, St. Mary Lake.

developed during this time. Both regions have been identified either by the presence of a thin cover of Paleozoic strata or by their absence altogether, indicating that these blocks were uplifted and, as a result, not buried by the deposition of sediments at that time. Furthermore, the region may have been affected by possible episodes of partial reheating from sediment loading related to deposition of Windermere and potentially Paleozoic strata, possible partial reheating associated with Cordilleran tectonic thickening in the Mesozoic, and possible partial reheating associated with Mesozoic magmatism. However, the degree to which each process or set of processes influenced the age spectra is difficult to assess.

Of the three samples in which duplicates were analyzed, the ages of ca. 78 and ca. 80 Ma for 17NR168-Ms from the KA

are within error of each other. On the other hand, ages for samples 17NR84-Ms and 17NR86 from the PA differ by more than 75 Ma (17NR84-Ms: ca. 674 and ca. 524 Ma; 17NR86: ca. 316 and ca. 240 Ma). Although it is possible that two generations of mica growth are present in sample 17NR84-Ms, there is no simple explanation as to why these aliquots yielded such different ages. Taking into consideration the wide spread of ages across the PA, in conjunction with the fact that samples from the KA yielded much younger, relatively flat reproducible spectra, it seems that the spread in ages across these two samples from the PA indicates that argon retentivity varies greatly in these samples, likely due to some combination of slow cooling and partial reheating. The inconsistent distribution of ages from across the PA is likely a regional-scale reflection of the variable ef-

fects of the different episodes of cooling and/or partial reheating.

The results of this study indicate that argon retention in biotite from rocks in the PA is unpredictable. Cooling ages from the PA range from 837 Ma to 240 Ma, with no systematic pattern of distribution (Figure 7). This observation most likely reflects variable degrees of resetting since the formation of the biotite in the Mesoproterozoic. Monotonically increasing age spectra indicate that some of the grains analyzed were subject to argon loss due to slow cooling. Additionally, sample 17NR14B from a previously undated, small granodioritic intrusive body returned a cooling age of 82 Ma from a monotonically increasing age spectrum that indicated final closure to ^{39}Ar loss at ca. 25 Ma. The interpreted cooling age for this sample overlaps with a population of cooling ages for intrusive rocks of the Bayonne magmatic suite (E. Webster, pers. comm., 2019). Localized domains of heating related to the emplacement of intrusions from the mid- to late-Cretaceous Bayonne magmatic suite may have led to partial reheating or partial resetting of $^{40}\text{Ar}/^{39}\text{Ar}$ cooling ages in rocks of the PA adjacent to the intrusions.

$^{40}\text{Ar}/^{39}\text{Ar}$ Ages in the Kootenay Arc

Across the portion of the field area that is occupied by the KA, the spread in cooling ages spans a much shorter time interval in comparison to the PA (139 to 55 Ma). The spectra for KA samples are defined by relatively flat release patterns, and the ages returned span the interval between regional metamorphism (144–134 Ma; Moynihan, 2012) and final exhumation (90–40 Ma; E. Webster, pers. comm., 2019) in this region.

Contrasts in Cooling Ages between the Purcell Anticlinorium and the Kootenay Arc

Interpretation of the results of this study, indicates that the PA and KA represent two different cooling domains. Interpretation of the geochronology data suggests that the PA appears to involve variable degrees of resetting of originally Mesoproterozoic cooling ages. The Neoproterozoic to latest Paleozoic/earliest Mesozoic cooling ages indicate that this region was never buried sufficiently, either through Neoproterozoic or Paleozoic sedimentation or Mesozoic Cordilleran tectonic thickening (folding and faulting) associated with the development of the PA, to uniformly exceed temperatures of approximately 300–400°C (closure temperature of argon in biotite and muscovite). For an average geothermal gradient of 30°C/km, this temperature corresponds to a depth of approximately 10–13 km. Conversely, cooling ages for the KA indicate that this portion of the study area was affected by Mesozoic Cordilleran tectonothermal processes between 139 and 55 Ma. In combination with the identification of the structural and metamorphic interface between the KA and PA, the implication is that an

important thermotectonic interface between the KA and PA existed at the time of Cordilleran tectonism. The PA, comprising a thick Mesoproterozoic stratigraphic package of turbidites and Moyie Sill, appears to have acted as a rigid backstop or ‘buttress’, perhaps to the east of a deep-crustal ramp, against which the elongate domain of thickening and Barrovian metamorphism in the KA was localized.

Conclusions

Deformation and metamorphism in the PA was widespread during the Mesoproterozoic and resulted in low-grade metamorphism and the development of an S_1 cleavage. The KA, on the other hand, was polydeformed and polymetamorphosed during the Mesozoic. Within the study area, the most conspicuous phases of Kootenay Arc-type deformation are D_2 , which resulted in a primary foliation (S_2), and deformation (D_3), which led to the development of upright folds, a crenulation cleavage, and regional-scale thrusting and folding of the PA. Evidence of structural modification and metamorphic mineral growth related to the D_2M_2 event is restricted to the northwestern portion of the field area, and dies out roughly 15 km east of the unconformity between the Windermere and Belt-Purcell supergroups. East of this interface, the observed deformation and metamorphism is ascribed to Mesoproterozoic processes.

New $^{40}\text{Ar}/^{39}\text{Ar}$ results for biotite and muscovite samples from rocks of the PA and eastern KA indicate that the two regions are also characterized by different cooling histories. The $^{40}\text{Ar}/^{39}\text{Ar}$ cooling ages for the PA span the interval from the Neoproterozoic to the latest Paleozoic/earliest Mesozoic (837–240 Ma). The nonsystematic distribution of ages across the PA indicates that this region was never deeply buried since the Mesoproterozoic and most likely experienced a multifaceted history of tectonothermal modification, including several episodes of uplift and erosion, sediment loading, crustal thickening and magmatism. Cooling ages for rocks of the KA, on the other hand, indicate that the region was affected by Cordilleran thickening, metamorphism and exhumation between 139 and 55 Ma. This contrast suggests that the PA may have acted as a relatively rigid buttress, against which the rocks of the KA were thickened and metamorphosed in the Mesozoic.

Acknowledgments

First and foremost, the authors would like to thank Geoscience BC for their support of this study. This work was funded by a Geoscience BC grant to D. Pattison and N. Rioseco, and a Natural Sciences and Engineering Research Council of Canada Discovery Grant to D. Pattison. They would also like to thank C. Padget, J. Forshaw and M. Lazzarotto of their insightful reviews of this manuscript.

References

- Anderson, H.E. and Davis, D.W. (1995): U-Pb geochronology of the Moyie sills, Purcell Supergroup, southeastern British Columbia: implications for the Mesoproterozoic geological history of the Purcell (Belt) basin; *Canadian Journal of Earth Sciences*, v. 32, p. 1180–1193, URL <<https://pubs.geoscienceworld.org/cjes/article-abstract/32/8/1180/52667>> [November 2019].
- Benvenuto, G.L. and Price, R.A. (1979): Structural evolution of the Hosmer thrust sheet, southeastern British Columbia; *Bulletin of Canadian Petroleum Geology*, v. 27, p. 360–394.
- Best, M., Christiansen, E.H., Deino, A.L., Gromme, C.S. and Tingey, D.G. (1995): Correlation and emplacement of a large, zoned, discontinuously exposed ash flow sheet; the $^{40}\text{Ar}/^{39}\text{Ar}$ chronology, paleomagnetism, and petrology of the Pahrangat Formation, Nevada; *Journal of Geophysical Research: Solid Earth*, v. 100, p. 24 593–24 609.
- Bishop, D.T. (1973): Petrology and geochemistry of the Purcell sills in Boundary country, Idaho and adjacent areas; *in* Proceedings of the Belt Symposium, Volume 2, D.T. Bishop (ed.), Idaho Bureau of Mines and Geology–Idaho University Department of Geology, Moscow, Idaho, Special Publication, p. 15–66.
- Dalrymple, B.G. and Lanphere, M.A. (1974): $^{40}\text{Ar}/^{39}\text{Ar}$ age spectra of some undisturbed terrestrial samples; *Geochimica et Cosmochimica Acta*, v. 38, p. 715–738.
- Dazé, A., Lee, J.K.W. and Villeneuve, M. (2003): An intercalibration study of the Fish Canyon sanidine and biotite $^{40}\text{Ar}/^{39}\text{Ar}$ standards and some comments on the age of the Fish Canyon Tuff; *Chemical Geology*, v. 199, p. 111–127.
- Deino, A.L. (2013): Users' manual for Mass Spec v7.961; Berkeley Geochronology Center, Berkeley, California, Special Publication 1a, 132 p.
- Deiss, C. (1941): Cambrian geology and sedimentation in the central Cordilleran region; *Bulletin of the Geological Society of America*, v. 52, p. 1085–1116, URL <https://pubs.geoscienceworld.org/gsa/gsabulletin/article-pdf/52/7/1085/3416174/BUL52_7-1085.pdf> [August 2019].
- DePaoli, G.R. and Pattison, D.R.M. (1995): Constraints on temperature-pressure conditions and fluid composition during metamorphism of the Sullivan orebody, Kimberley, British Columbia, from silicate-carbonate equilibria; *Canadian Journal of Earth Sciences*, v. 32, p. 1937–1949, URL <<https://doi.org/10.1139/e95-148>> [September 2019].
- Devlin, W.J. and Bond, G.C. (1988): The initiation of the early Paleozoic Cordilleran miogeoclinal: evidence from the uppermost Proterozoic–Lower Cambrian Hamill Group of southeastern British Columbia; *Canadian Journal of Earth Sciences*, v. 25, p. 1–19, URL <<https://doi.org/10.1139/e88-001>> [September 2019].
- Devlin, W.J., Brueckner, H.K. and Bond, G.C. (1988): New isotopic data and a preliminary age for volcanics near the base of the Windermere Supergroup, northeastern Washington, USA; *Canadian Journal of Earth Sciences*, v. 25, p. 1906–1911, URL <<http://doi.org/10.1139/e88-179>> [August 2019].
- Doughty, P.T. and Chamberlain, K.R. (1996): Salmon River Arch revisited: new evidence for 1370 Ma rifting near the end of deposition in the Middle Proterozoic Belt basin; *Canadian Journal of Earth Sciences*, v. 33, p. 1037–1052, URL <<https://doi.org/10.1139/e96-079>> [October 2019].
- Evans, K.V., Aleinikoff, J.N., Obradovich, J.D. and Fanning, C.M. (2000): SHRIMP U-Pb geochronology of volcanic rocks, Belt Supergroup, western Montana: evidence for rapid deposition of sedimentary strata; *Canadian Journal of Earth Sciences*, v. 37, p. 1287–1300, URL <<https://doi.org/10.1139/e00-036>> [October 2019].
- Fyles, J.T. (1964): Geology of the Duncan Lake area, Lardeau District, British Columbia; BC Ministry of Energy, Mines and Petroleum Resources, BC Geological Survey, Bulletin 49, 87 p., URL <http://cmscontent.nrs.gov.bc.ca/geoscience/PublicationCatalogue/Bulletin/BCGS_B049.pdf> [June 2019].
- Ghosh, D.K. (1995): U-Pb geochronology of Jurassic to early Tertiary granitic intrusives from the Nelson–Castlegar area, southeastern British Columbia, Canada; *Canadian Journal of Earth Sciences*, v. 32, p. 1668–1680, URL <<https://doi.org/10.1139/e95-132>> [October 2019].
- Höy, T. (1989): The age, chemistry, and tectonic setting of the Middle Proterozoic Moyie sills, Purcell Supergroup, southeastern British Columbia; *Canadian Journal of Earth Sciences*, v. 26, p. 2305–2317, URL <<https://doi.org/10.1139/e89-196>> [June 2019].
- Kuiper, K.F., Deino, A., Hilgen, F.J., Krijgsman, W., Renne, P.R. and Wijbrans, J.R. (2008): Synchronizing rock clocks of Earth history; *Science*, v. 320, p. 500–504, URL <<https://doi.org/10.1126/science.1154339>> [October 2019].
- Lanphere, M.A. and Dalrymple, B.G. (1976): Identification of excess ^{40}Ar by the $^{40}\text{Ar}/^{39}\text{Ar}$ age spectrum technique; *Earth and Planetary Science Letters* v. 32, p. 141–148, URL <[https://doi.org/10.1016/0012-821X\(76\)90052-2](https://doi.org/10.1016/0012-821X(76)90052-2)> [August 2019].
- Larson, K.P., Camacho, A., Cottle, J.M., Coutand, I., Buckingham, H.M., Ambrose, T.K. and Rai, S.M. (2017): Cooling, exhumation, and kinematics of the Kanchenjunga Himal, far east Nepal; *Tectonics*, v. 36, p. 1037–1052, URL <<https://doi.org/10.1002/2017TC004496>> [November 2019].
- Lee, J.K.W., Onstott, T.C., Cashman, K.V., Cumbest, R.J. and Johnson, D. (1991): Incremental heating of hornblende in vacuo: implications for $^{40}\text{Ar}/^{39}\text{Ar}$ geochronology and the interpretation of thermal histories; *Geology*, v. 19, p. 872–876, URL <<https://pubs.geoscienceworld.org/gsa/geology/article-pdf/19/9/872/3512548/i0091-7613-19-9-872.pdf>> [October 2019].
- Leech, G.B. (1962): Metamorphism and granitic intrusions of Precambrian age in southeast British Columbia; *Geological Survey of Canada, Paper 62-13*, 11 p., URL <<https://doi.org/10.4095/101124>> [November 2019].
- Logan, J.M. (2001): Prospective areas for intrusion-related gold-quartz veins in southern British Columbia; *in* Geological Fieldwork 2000, BC Ministry of Energy, Mines and Petroleum Resources, BC Geological Survey, Paper 2001-1, p. 231–252.
- Ludwig, K.R. (2008): User's manual for ISOPLOT 3.60: a geochronological toolkit for Microsoft Excel; Berkeley Geochronology Center, Special Publication 4, 54 p.
- Lund, K., Aleinikoff, J.N., Evans, K. V. and Fanning, C.M. (2003): SHRIMP U-Pb geochronology of Neoproterozoic Windermere Supergroup, central Idaho: implications for rifting of western Laurentia and synchronicity of Sturtian glacial deposits; *Bulletin of the Geological Society of America*, v. 115, p. 349–372, URL <<https://doi.org/10.1130/>

- 0016-7606(2003)115<0349:SUPGON>2.0.CO;2> [June 2019].
- McDougall, I. and Harrison, T.M. (1999): *Geochronology and Thermochronology by the $^{40}\text{Ar}/^{39}\text{Ar}$ Method* (2nd edition); Oxford University Press, New York, New York, 269 p.
- McFarlane, C.R.M. (2015): A geochronological framework for sedimentation and Mesoproterozoic tectono-magmatic activity in lower Belt-Purcell rocks exposed west of Kimberley, British Columbia; *Canadian Journal of Earth Sciences*, v. 52, p. 444–465, URL <<https://doi.org/10.1139/cjes-2014-0215>> [October 2019].
- McMechan, M.E. and Price, R.A. (1982): Superimposed low-grade metamorphism in the Mount Fisher area, southeastern British Columbia – implications for the East Kootenay orogeny; *Canadian Journal of Earth Sciences*, v. 19, p. 476–489, URL <<https://doi.org/10.1139/e82-039>> [October 2019].
- Moynihan, D.P. (2012): *Metamorphism and Deformation of the Central Kootenay Arc, southeastern British Columbia*; Ph.D. thesis, University of Calgary, 279 p.
- Moynihan, D.P. and Pattison, D.R.M. (2013): Barrovian metamorphism in the central Kootenay Arc, British Columbia: petrology and isograd geometry; *Canadian Journal of Earth Sciences*, v. 50, p. 769–794, URL <<https://doi.org/10.1139/cjes-2012-0083>> [October 2019].
- Norris, D.K. and Price, R.A. (1966): Middle Cambrian lithostratigraphy of southeastern Canadian Cordillera; *Bulletin of Canadian Petroleum Geology*, v. 14, p. 385–404.
- Pattison, D.R.M. and Seitz, J.D. (2012): Stabilization of garnet in metamorphosed altered turbidites near the St. Eugene lead-zinc deposit, southeastern British Columbia: equilibrium and kinetic controls; *Lithos*, v. 134–135, p. 221–235, URL <<https://doi.org/10.1016/j.lithos.2011.12.007>> [October 2019].
- Price, R.A. (1984): Tectonic evolution of the Purcell (Belt) rocks of the southeastern Canadian Cordillera and adjacent parts of the United States; *in* The Belt, W. Hobbs (ed.), *Belt Symposium II 1983*, Montana Bureau of Mines and Geology, abstracts and summaries, Special Publication 90, p. 47–48.
- Price, R.A. (2000): The southern Canadian Rockies: evolution of a foreland thrust and fold belt; *GeoCanada 2000*, Calgary, May 29–June 2, 2000, Field Trip Guidebook no. 13, 246 p., URL <<https://doi.org/10.13140/2.1.2910.2887>> [September 2019].
- Renne, P.R. and Norman, E.B. (2001): Determination of the half-life of ^{37}Ar by mass spectrometry; *Physical Review C*, v. 63, 3 p., URL <<https://doi.org/10.1103/PhysRevC.63.047302>> [August 2019].
- Renne, P.R., Swisher, C.C., Deino, A.L., Karner, D.B., Owens, T.L. and DePaolo, D.J. (1998): Intercalibration of standards, absolute ages and uncertainties in $^{40}\text{Ar}/^{39}\text{Ar}$ dating; *Chemical Geology*, v. 145, p. 117–152, URL <[https://doi.org/10.1016/S0009-2541\(97\)00159-9](https://doi.org/10.1016/S0009-2541(97)00159-9)> [August 2019].
- Rioseco, N.A. and Pattison, D.R.M. (2018): Preliminary investigations of the metamorphic and thermochronological interface between the Purcell Anticlinorium and the Kootenay Arc, southeastern British Columbia (NTS 082F, G); *in* *Geoscience BC Summary of Activities 2017: Minerals and Mining*, Geoscience BC, Report 2018-01, p. 47–56, URL <http://www.geosciencebc.com/i/pdf/SummaryofActivities2017/MM/SoA2017_MM_Rioseco.pdf> [November 2019].
- Rioseco, N.A., Pattison, D.R.M. and Ashton, R.E. (2019): The Relationship between Deformation and Metamorphism in the Interface between the Purcell Anticlinorium and the Kootenay Arc, southeastern British Columbia (NTS 082F, G); *in* *Geoscience BC Summary of Activities 2018: Minerals and Mining*, Geoscience BC, Report 2019-01, p. 1–14, URL <http://cdn.geosciencebc.com/pdf/SummaryofActivities2018/MM/2017-009_SoA2018_MM_Rioseco.pdf> [November 2019].
- Roddick, J.C. (1983): High precision intercalibration of ^{40}Ar - ^{39}Ar standards; *Geochimica et Cosmochimica Acta*, v. 47, p. 887–898, URL <[https://doi.org/10.1016/0016-7037\(83\)90154-0](https://doi.org/10.1016/0016-7037(83)90154-0)> [August 2019].
- Ross, J. (2017): PChron software, URL <<https://doi.org/10.5281/zenodo.9884>> [November 2019].
- Sears, J.W., Chamberlain, K.R. and Buckley, S.N. (1998): Structural and U-Pb geochronological evidence for 1.47 Ga rifting in the Belt basin, western Montana; *Canadian Journal of Earth Sciences*, v. 35, p. 467–475, URL <<https://doi.org/10.1139/e97-121>> [September 2019].
- Spell, T.L. and McDougall, I. (2003): Characterization and calibration of $^{40}\text{Ar}/^{39}\text{Ar}$ dating standards; *Chemical Geology*, v. 198, p. 189–211, URL <[https://doi.org/10.1016/S0009-2541\(03\)00005-6](https://doi.org/10.1016/S0009-2541(03)00005-6)> [August 2019].
- Steiger, R.H. and Jager, E. (1977): Subcommittee on geochronology: convention on the use of decay constants in geo- and cosmochronology; *Earth and Planetary Science Letters*, v. 36, p. 359–362.
- Warren, M.J. (1997): *Crustal extension and subsequent crustal thickening along the Cordilleran rifted margin of ancestral North America, western Purcell Mountains, southeastern British Columbia*; Ph.D. thesis, Queen's University, 360 p.
- Webster, E.R. and Pattison, D.R.M. (2018): Spatially overlapping episodes of deformation, metamorphism, and magmatism in the southern Omineca Belt, southeastern British Columbia; *Canadian Journal of Earth Sciences*, v. 55, p. 84–110, URL <<https://doi.org/10.1139/cjes-2017-0036>> [October 2019].
- Webster, E.R., Pattison, D.R.M. and DuFrane, S.A. (2017): Geochronological constraints on magmatism and polyphase deformation and metamorphism in the southern Omineca; *Canadian Journal of Earth Sciences*, v. 54, p. 529–549, URL <<https://doi.org/10.1139/cjes-2016-0126>> [August 2019].